



# Isothermal Aging Effect on Sn-58Bi Solder Interconnect Mechanical Shear Stability

Gihan Dodanduwa Waduge<sup>1</sup> · Greg Baty<sup>1</sup> · Young-woo Lee<sup>2</sup> · Tae-Kyu Lee<sup>3</sup>

Received: 25 August 2021 / Accepted: 30 November 2021 / Published online: 2 January 2022  
© The Minerals, Metals & Materials Society 2021

## Abstract

Use of low melting temperature solder (LTS) materials in interconnect devices is a recent application as they lower the challenges of high reflow peak temperature-induced package warpage during assembly. A good candidate to overcome this challenge is a eutectic Sn-Bi system solder, with a melting temperature of 138°C and a reflow peak assembly temperature of around 185°C. However, Bi causes joint hardening and is prone to brittle fractures under mechanical bend and shock. Therefore, it is critical to understand mechanical properties of Sn-58Bi solder joints under conditions of end-use condition and applications. In this study, a series of isothermally aged 300- $\mu$ m-diameter solder balls attached to a NiAu pad surface finish, are subject to single-ball shear tests after up to 500 h aging at room temperature, 100°C and –25°C. Single-ball shear tests were performed using a multi-bond tester with 10- $\mu$ m shear height and two shear speed condition, 10  $\mu$ m/s and 100  $\mu$ m/s. The maximum shear load and the distance to the peak shear load were measured to observe the deformation behavior change. Comparative testing was also conducted for Sn-1.0Ag-0.5Cu (wt.%) aged samples for comparison. A decrease in maximum shear strength and loss of ductility with 100°C isothermal aging, opposite to an increase in ductility with room temperature isothermal aging were observed. Isothermally aged Sn-58Bi samples reveal further loss of ductility compared to SAC105 which show increase in ductility. This phenomenon is due to the increased Bi solubility into Sn at a higher temperature range. The deformation behavior for both Sn-58Bi and SAC105 were observed and discussed on partially sheared solder joints using EBSD analysis.

**Keywords** Isothermal aging · low melting temperature solder · Sn-58Bi · single-ball shear · microstructure

## Introduction

Modern electronics require miniaturized devices but with more complex configuration and higher power and higher density interconnects; consequently, an increasing number of chips and functionality in a given substrate.<sup>1</sup> Heterogeneous integration through SIP (system-in-package) can leverage these requirements of packaging technology to create multiple functions associated with a system or subsystem.<sup>2</sup> However, the recent technology associated with these complex devices causes temperature variations and thermally

induced stresses to arise from the dissimilar coefficients of thermal expansion (CTE) of packaging materials. This, in turn, causes interconnect reliability degradation, and eventually compromises the functionality of the whole packaging assembly.<sup>3</sup> Along with complexity a package needs an increase in substrate and body size, which poses a constant challenge to the board assembly process due to the package warpage.<sup>3</sup> As a possible solution to these challenges, low temperature solder (LTS) interconnects are of considerable interest and in development, which primarily focuses on reducing energy consumption for a lower carbon footprint and also results in lower thermal stresses and reduced defect rate, such as reducing dynamic warpage in large body size SIP systems, thereby improving solder joint quality and yield.<sup>4,5</sup> Among LTS alloys, Sn-based alloy systems including Sn-In or Sn-Bi binary-based alloys are under consideration with additional elements such as Ag, Sb, In and Co.<sup>6</sup> Eutectic Sn-Bi binary metallurgical systems are an obvious option due to their lower melting temperature around 138°C,

✉ Tae-Kyu Lee  
taeklee@cisco.com

<sup>1</sup> Department of Mechanical and Materials Engineering, Portland State University, Portland, OR, USA

<sup>2</sup> MK Electron, Seoul, Korea

<sup>3</sup> Cisco Systems, San Jose, CA, USA

and other advantages of Sn–Bi-based solder are that it is associated with sufficient solderability, mechanical properties, joint strength, creep resistance, low coefficient of thermal expansion, and relatively low cost.<sup>7–10</sup>

However, in general, Sn–Bi systems showed a few performance challenges, which can be a deterrent for their use in electronics device interconnects. As shown in the phase diagram in Fig. 1a, the Bi solubility into the Sn varies from 2% to 10% at room temperature and 100°C respectively, depending on the holding temperature. Unlike the ductile deformation behavior in similar eutectic Sn–Pb systems, Sn–58Bi exhibits a brittle behavior due to the Bi crystal structure difference at elevated temperature conditions.<sup>11</sup> As displayed in Fig. 1b, bismuth's inherently brittle nature is largely attributed to its rhombohedral crystal structure, with two bilayers within its hexagonal structure, and very few of the slip planes that are necessary for material ductility.<sup>12</sup> In fact, bismuth has only one third the slip planes found in Sn and one sixth the slip planes found in Cu, Ni, Al and Pb.<sup>13,14</sup> Bi-containing Sn alloys have been established to undergo extensive  $\beta$ -Sn recrystallization after aging, caused by precipitation of homogeneously distributed Bi precipitates.<sup>15</sup> Furthermore, isothermal aging causes more Bi coarsening by inducing precipitation of oversaturated Bi, in which the precipitated Bi particles can attach to the previously formed Bi-rich phases, leading to growth of the coarsened Bi phases via thermally activated diffusion.<sup>16</sup> A recent study on low melting temperature interconnect behavior showed that isothermal aging at 100°C for 200 h decreased the maximum shear strength further and increased the brittle behavior in Sn–58Bi.<sup>17</sup> Therefore, it has become important to establish the impact of this brittle behavior under isothermal aging

using various temperatures identifying degradation mechanisms and which mechanisms are key to improving mechanical performance. At the same time, it remains important to determine an experimental approach that could potentially be identified in order to overcome the inherent brittleness of the eutectic Sn–Bi solder composition. By performing instantaneous mechanical shear load tests on single solder balls with different aging temperatures and holding time, a better understanding of solder interconnect stability can be obtained. In this study, maximum shear force measurements applied on single solder balls, comparing isothermally aged Sn–58Bi and SAC105 single-joint solders after aging at room temperature, 100°C and –25°C were performed using a multi-bond tester with 10  $\mu\text{m/s}$  and 100  $\mu\text{m/s}$  shear speed. Along with shear tests, the microstructural investigations were carried out using scanning electron microscopy (SEM), electron backscattered diffraction (EBSD) and energy dispersive spectrometry (EDS) to observe the stress and strain levels associated with the fracture and crack propagation path.

## Experimental Procedure

Figure 2 shows the initial SEM and corresponding EBSD images of unaged and 100°C/500 h aging conditions for SAC105 and Sn–58Bi. The 100°C aging condition did not induce much microstructure change between the unaged and aged SAC105 sample, but vastly transformed the Sn–58Bi microstructure. As shown in Fig. 2c and d, the eutectic Sn–58Bi resulted in both Sn and Bi grain growth from an average grain size of 0.3  $\mu\text{m}$  to 1  $\mu\text{m}$ . Because of the large grain

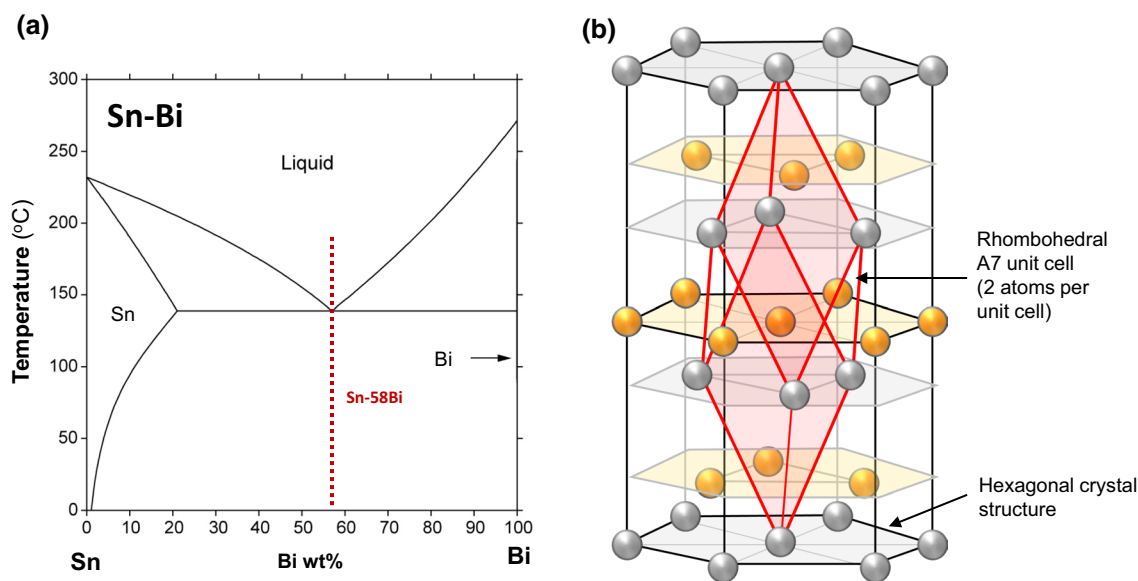


**Fig. 1** (a) Sn–Bi binary phase diagram and (b) schematic of hexagonal crystal structure of bulk bismuth (Bi).

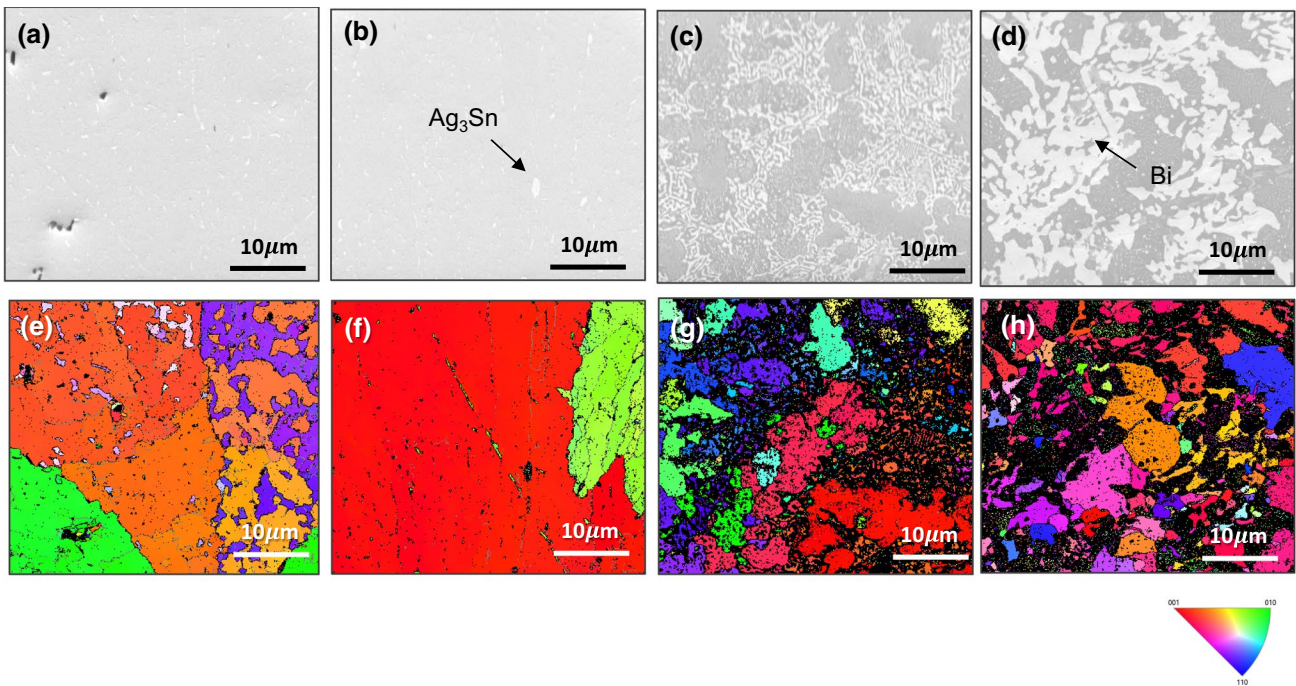


**Fig. 2** Scanning electron microscope image (a, b, c, d) and corresponding EBSD inverse pole figure (IPF) (e, f, g, h) for SAC105 before aging (a, e) and after aging at 100°C/500 h (b, f). Sn-58Bi before aging (c, g) and after aging at 100°C/500 h (d, h).

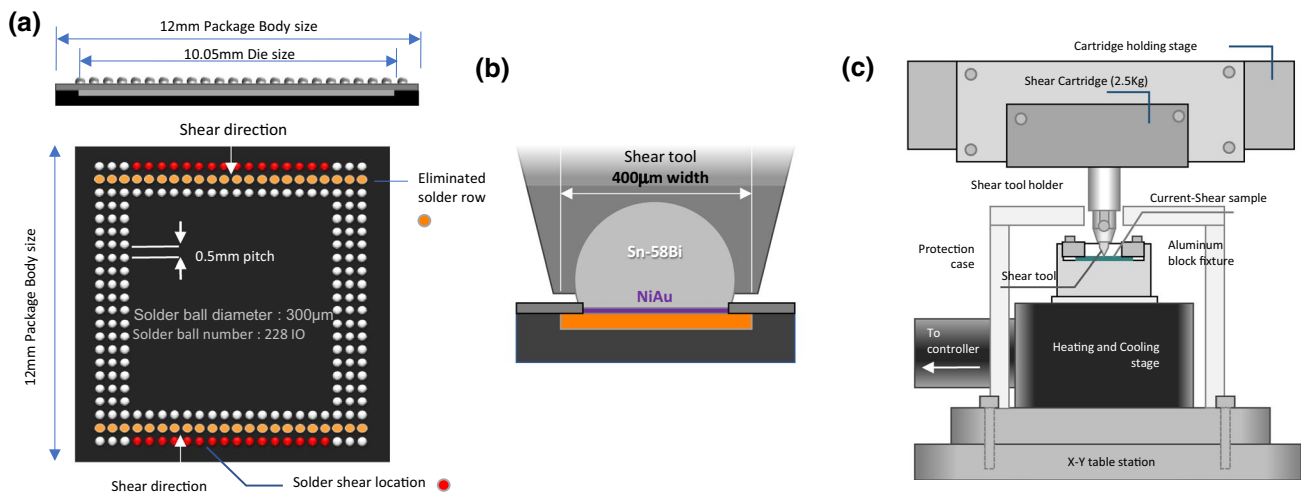


**Fig. 3** Test vehicle and single solder ball shear test set-up. (a) BGA test component, (b) ball shear tool and solder ball configuration front view and (c) shear tester schematic set-up with heating and cooling stage.

size distribution, Sn-58Bi is expected to have a property change associated with isothermal aging at 100°C. The test configuration used in this study is presented in Fig. 3. As shown in Fig. 3a, 12 × 12 mm ball grid arrays (BGAs) with a three-row perimeter was used in this study with 228 total solder balls per component. The second row of solder balls were removed from the edge solder array to provide a clearance for the first-row solder ball shearing. The substrates of

the package side had an electrolytic Ni/Au surface finish on top of the Cu pad. The solder balls used in this study were composed of SAC105 and Sn-58Bi solder balls with diameters of 300 µm positioned with 0.5-mm pitch. The solder ball configuration and schematic shear tool configuration are shown in Fig. 3b with dimensions. The width of the shear tool used was 400 µm. All shear tests were performed at a 10-µm shear height, and shear speed of either 10 µm/s

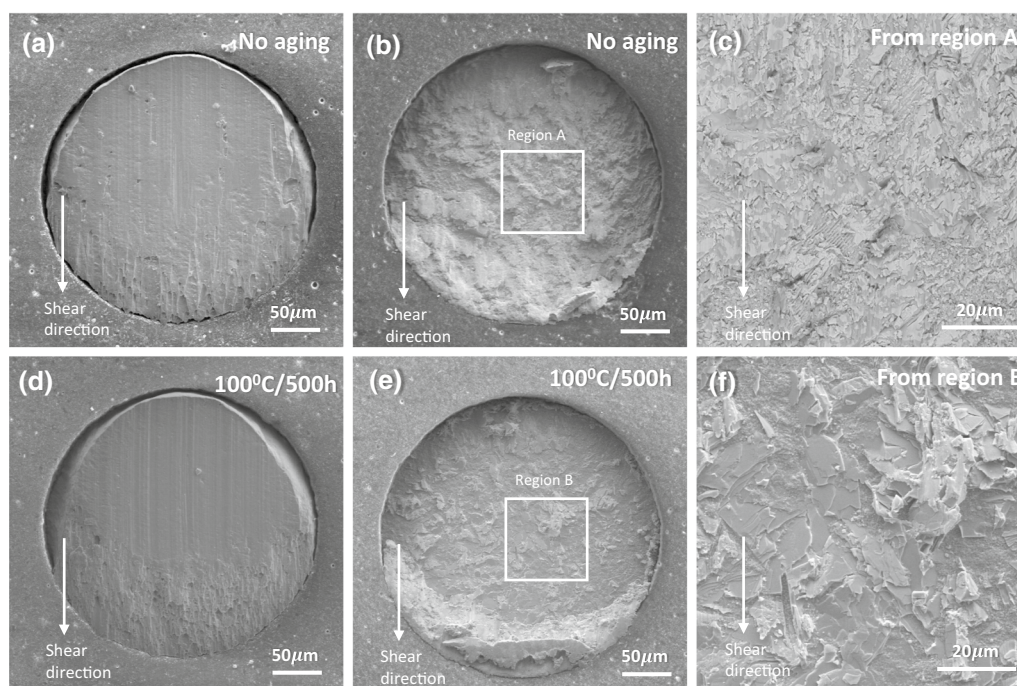


or 100  $\mu\text{m/s}$ . This shear height was chosen based on the results of a previous study with expanded shear testing at various shear heights.<sup>18</sup> When accumulating the data from this experiment, it is significant to note that some of the shear curves were found to start somewhat after traveling, meaning shear began at 10  $\mu\text{m}$  instead of at 0 distance. This was simply fixed by subtracting the starting difference from the peak load to generate the starting point distance to peak load distance. To perform the shear test, a Nordson Dage 4000 plus multi-bond tester was used (Fig. 3c). All shear tests were performed at room temperature after isothermal aging at 25°C, 100°C and -25°C for 50 h, 100 h, 200 h and 500 h to compare with the non-aged sample configuration. Isothermally aged samples were moved from the thermal chambers to the multi-bond tester before the shear test. To maintain the shear test at constant temperature, the cooling and heating stage was used to bring the sample to room temperature either by heating and cooling per isothermal condition. The cooling rate from 100°C aging condition to room temperature was around  $\sim 70^\circ\text{C}/\text{min}$ . Microstructure analysis was completed on samples through cross sectioning and observation using an FEI Sirion XL30 scanning electron microscope (SEM). The SEM was equipped with an Oxford Instruments electron backscatter diffraction detector (EBSD), allowing further analysis of the crack propagation path, fracture surface and localized strain and stress

via strain contour and grain reference orientation deviation (GROD) maps.

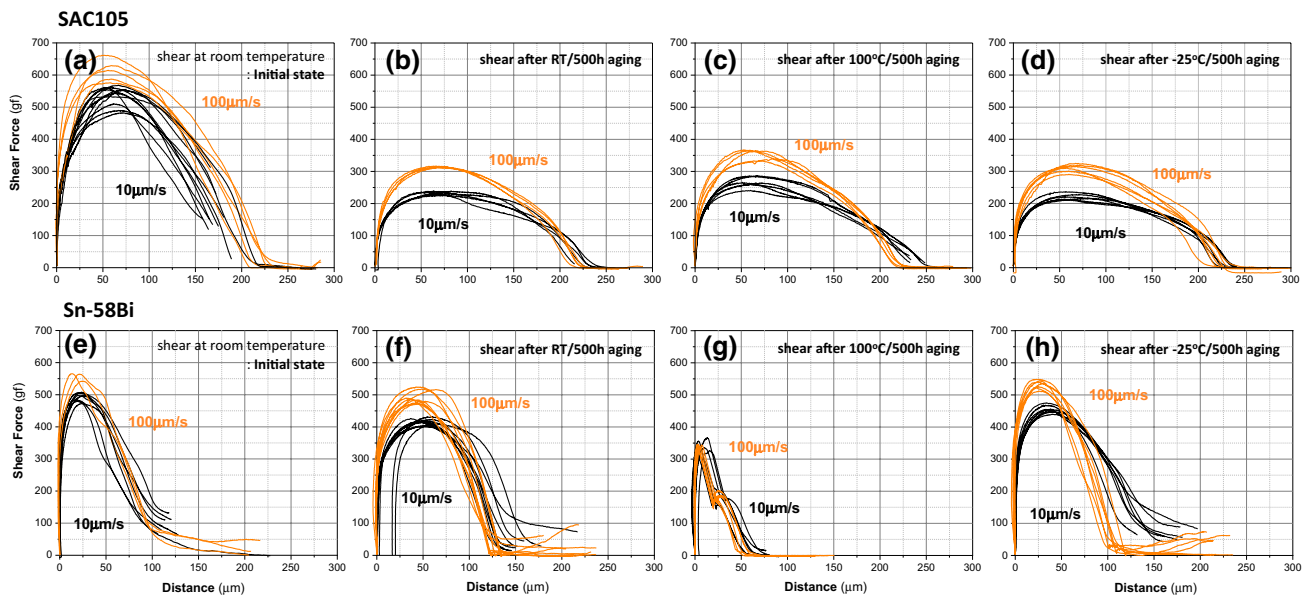
## Results and Discussion

Figure 4 shows the SEM fracture surface images for the SAC105 (Fig. 4a and d) and Sn-58Bi (Fig. 4b and e) solder-to-pad interface after shearing at room temperature with and without 100°C/500 h aging. The crack propagates in the SAC105 bulk region leaving a ductile fracture mode surface for both unaged and 100°C isothermally aged samples but with a small variation in the maximum shear load per isothermal aging condition which can be observed in the maximum shear load distribution curves in Fig. 5. The associated fracture surface image for the unaged Sn-58Bi (Fig. 4b) reveals that the majority of the sheared surface area contained a mixture of ductile fractured Sn-rich and brittle fractured Bi-rich regions. High-magnification SEM image from the white box (region A) is shown in Fig. 4c, which identifies the localized ductile and brittle mixed region. Compared to the non-aged sample, the Sn-58Bi sheared sample in Fig. 4e aged at 100°C exhibits a dominant brittle surface fracture as the majority of the fracture surface contained small islands of residual Sn and a predominance of Bi-rich phase, which can be seen in the high magnification SEM image with a mixture of trans-granular cracks (region



**Fig. 4** Fracture surface SEM images of SAC105 (a, b, c, d) and SnBi (b, c, d, e) solder joint after shear test with 100 mm/s shear speed per aging condition. (a) and (b) Shear test after no aging; (d) and (e)

shear test after 100°C/500 h aging. (c) and (f) High-magnification of region A and region B.



**Fig. 5** Shear curves of shear speeds 10  $\mu\text{m/s}$  and 100  $\mu\text{m/s}$  for SAC105 (a, b, c, d) and Sn-58Bi (e, f, g, h). (a) and (e) Shear at room temperature right after ball attachment, isothermally aged at room

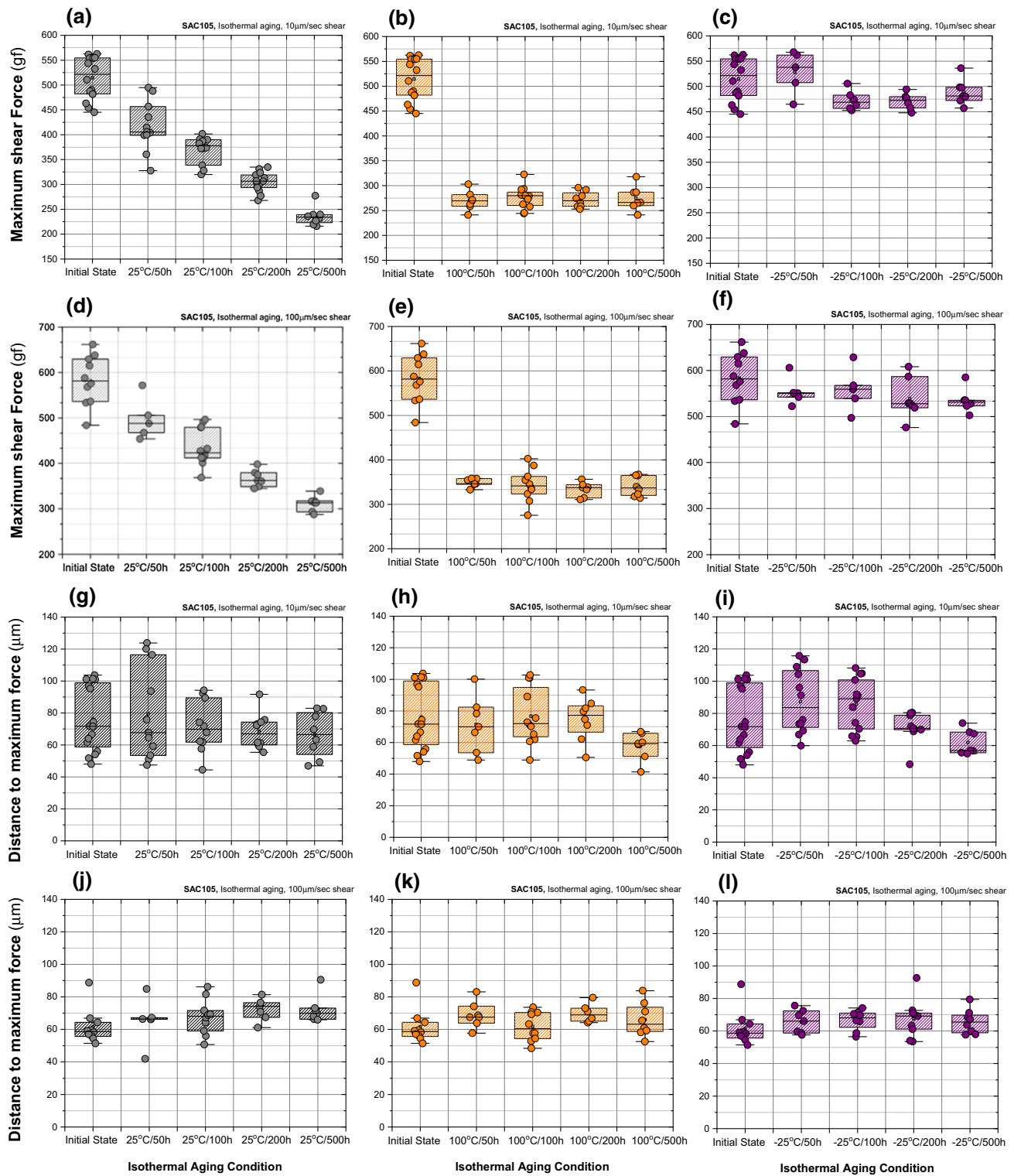
temperature (b, f), shear after 100°C/500 h (c, g), and shear after -25°C/500 h aging (d, h).

B) in Fig. 4f. Besides this brittle fracture occurring inside the bulk solder region, preferentially, there are fractures also occurring at the interface layer region, mainly near Sn to Bi grain boundary where Bi diffused and dissolved into Sn grains in which the interface mostly identified as extremely brittle.

Figure 5 presents a series of accumulated shear test curves for SAC105 (Fig. 5a, b, c, and d) and Sn-58Bi (Fig. 5e, f, g, and h) for isothermal aging pre-conditions and shear speed. Single solder ball shear curves for non-aged samples for 10  $\mu\text{m/s}$  and 100  $\mu\text{m/s}$  shear speed are presented in Fig. 5a and e representing the initial condition followed by isothermally aged shear data at room temperature (Fig. 5b and f), 100°C (Fig. 5c and g), and -25°C (Fig. 5d and h), respectively. Non-aged solder balls tested at room temperature for both SAC105 and Sn-58Bi showed the highest shear load value, which then decreased with longer isothermal aging. This downward shift of curves for both shear speeds is quite visible in SAC105 compared to eutectic Sn-58Bi. Also observed is the distance to the peak shear force, which indicates the ductility of the solder ball shear behavior. Compared to the initial state distance to the peak shear force, the isothermally aged solder ball shear results maintained ductility, which is also shown in Fig. 6g, h, i, j, k and l for both 10 and 100  $\mu\text{m/s}$  shear speed conditions. But shown in Fig. 5e, f, g, and h, Sn-58Bi indicates a different trend for isothermal aging. The decrease in maximum shear force is similar to SAC105, but the distance to peak shear force increased with room temperature aging (Fig. 5f) and decreased with

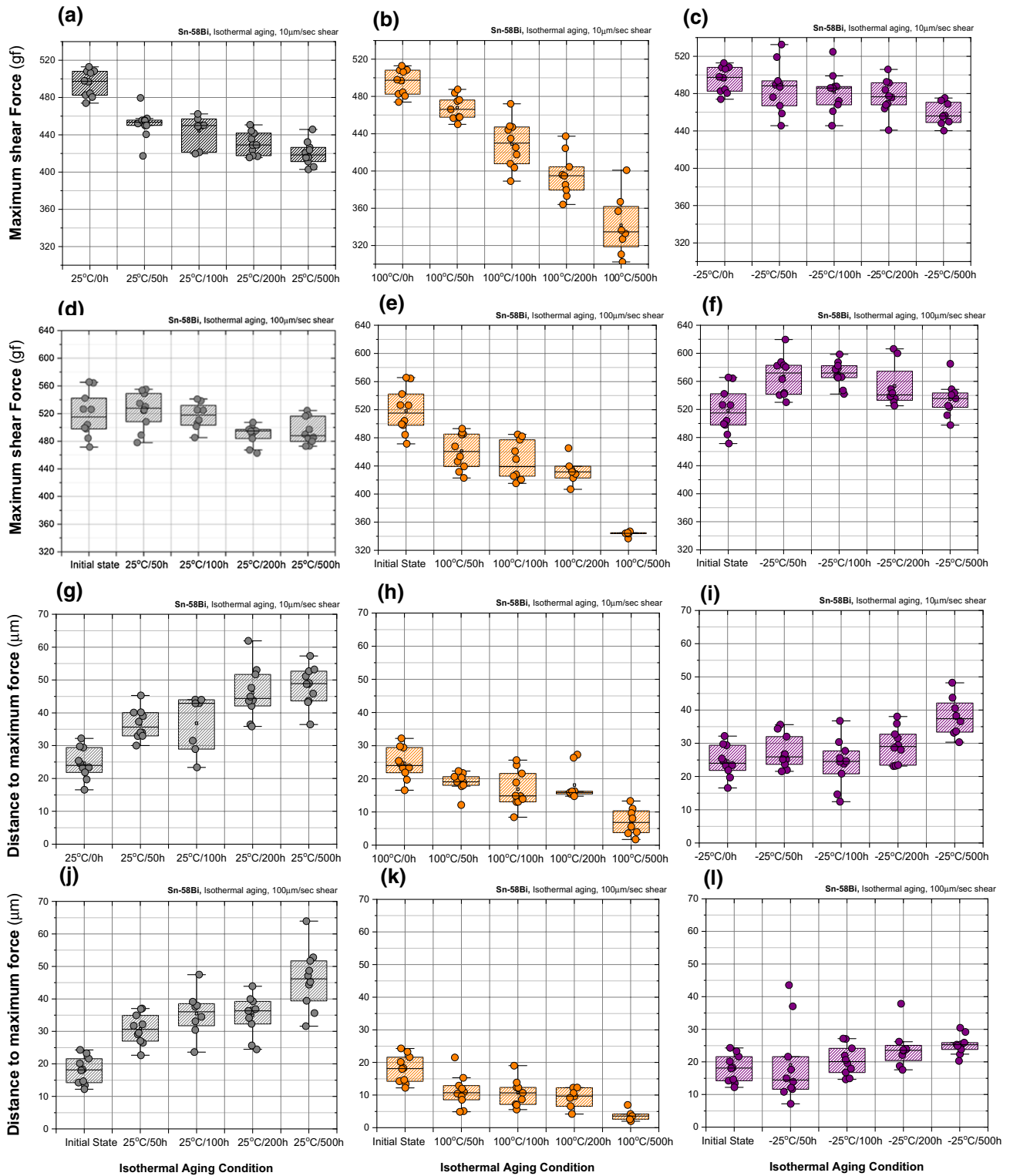
100°C aging (Fig. 5g). Especially significant is the decrease in distance to peak shear force with 100°C aging, which means that the brittleness increased significantly with aging. On the other hand, the room temperature aging after 500 h increased the ductility which is also shown in Fig. 7g and j. The shear test results at -25°C aged samples in Fig. 5h showed a similar trend of load-distance behavior as room temperature aged conditions with a gradual decrease in shear load after the peak shear load but at a slower rate. All maximum shear force data points per given conditions are presented in Figs. 6 and 7 for both SAC105 and Sn-58Bi. The variations of SAC105 plots in Fig. 6 were then compared to that of Sn-58Bi (Fig. 7).

Figure 6 presents the alloy SAC105 plots of maximum shear load values for isothermal aging at 10  $\mu\text{m/s}$  (Fig. 6a, b, and c) and 100  $\mu\text{m/s}$  (Fig. 6d, e, and f) shear speeds followed by corresponding plots of distance to peak shear force value (Fig. 6g, h, i, j, k, and l) for the same aging conditions. As mentioned in the explanation for Fig. 5, SAC105 showed the highest maximum shear force at the initial state, which is right after the ball attachment process. The isothermal aging condition at room temperature shown in Fig. 6a, b, c, and d revealed a continuous downward trend with longer aging time. In contrast, maximum shear force values of 100°C samples dropped abruptly to the range between 250 gf and 300 gf from initial condition of 550 gf and then continued on to maintain a constant level (Fig. 6b and e). The 100°C aging brought the maximum shear force to a saturated lower force level more quicker than the room temperature aging, but



**Fig. 6** SAC105 maximum shear force distribution for shear speeds 10  $\mu\text{m}/\text{s}$  (a, b, c), 100  $\mu\text{m}/\text{s}$  (d, e, f) and distance to maximum peak force for shear speeds 10  $\mu\text{m}/\text{s}$  (g, h, i) and 100  $\mu\text{m}/\text{s}$  (j, k, l). Isothermal

aging at room temperature (a, d, g, j), after aging at 100°C (b, e, h, k) and aging at -25°C (c, f, i, l).



**Fig. 7** Sn-58Bi maximum shear force distribution for shear speeds 10  $\mu\text{m}/\text{s}$  (a, b, c), 100  $\mu\text{m}/\text{s}$  (d, e, f) and distance to maximum peak force for shear speeds 10  $\mu\text{m}/\text{s}$  (g, h, i) and 100  $\mu\text{m}/\text{s}$  (j, k, l). Isothermal aging at room temperature (a, d, g, j), after aging at 100°C (b, e, h, k) and aging at -25°C (c, f, i, l).



with  $-25^{\circ}\text{C}$  aging condition, the maximum shear force did not decrease as much as the samples aged at room temperature and  $100^{\circ}\text{C}$ . The associated distance to peak shear force plots are presented in Fig. 6g, h, i, j, k, and l per condition. Unlike a downward trend in maximum shear force values, the distance to peak force, which represents the ductility if the solder ball maintained its level regardless of the aging condition. In an earlier publication, it was found that during a ball attachment reflow, Ni diffused from substrate into the solder bulk region, forming  $(\text{Cu,Ni})_6\text{Sn}_5$  at the solder to the Ni interface, which became thicker at the interface due to aging at  $150^{\circ}\text{C}$ .<sup>14</sup> However, the sheared samples aged at  $-25^{\circ}\text{C}$  exhibited a similar value of shear strength to the room temperature initial conditions in both strain rates at all aging conditions, indicating the alloy's ability to mitigate degradation even with longer aging (Fig. 6c and f). The distance to maximum shear force curves (Fig. 6g, h, i, j, k, and l) reveal that among the three temperature conditions with respect to two strain rates, there were not significant differences in the changing of ductility behavior with aging.

The SAC105 shear test results for the isothermal condition are compared to the shear behavior for Sn-58Bi in Fig. 7. The downward trend with longer aging time resembles the behavior of the SAC105 maximum shear force, but demonstrates a different behavior associated with the distance to the peak force. The distance to the peak force value increased with longer aging time at room temperature, as shown in Fig. 7g, h, i, and j, which is a different upward trend compared to the SAC105 behavior shown in Fig. 6g, h, i, and j. It also shows that the ductility is increased with longer aging time at room temperature. But at the same time the ductility decreased with longer aging time at  $100^{\circ}\text{C}$ , as shown in Fig. 7h, i, j, and k. This indicates that Sn-58Bi gained ductility with room temperature aging and, conversely, lost ductility with longer aging time at  $100^{\circ}\text{C}$ . This demonstrates that thermal aging can change the behavior of Sn-58Bi solders. The reasoning behind this trend is the limited Bi diffusivity towards the intermetallic compound (IMC) at the interface region and the increased Bi solubility into the Sn-rich grains at the grain boundaries between Bi and Sn. Since Bi is not reacting with IMC at the interface region, only Sn will be consumed by the IMC growth leaving the Bi not absorbed into the IMC but retained near the IMC-to-solder interface. This makes the interface more prone to brittle fracture which was observed at the fracture surface after  $100^{\circ}\text{C}$  aging shown in Fig. 4e and f. The loss of ductility is also observed in the shear plots shown in Fig. 5g and the associated shear force and distance to peak shear force in Fig. 7b, e, h and k. An additional reason for this downward trend of shear force and the loss of ductility is the increased Bi solubility at higher temperature. As shown in Fig. 1a, the Bi solubility into Sn at  $100^{\circ}\text{C}$  is more than 10 wt.% compared to the solubility at room temperature. The

continuous diffusion of Bi into Sn resulted a solid solution hardening near the Sn and Bi grain boundary and caused loss of ductility. On the contrary, the room temperature aging allows Bi, which was over saturated in Sn during solidification, to diffuse back into the Bi-rich grains due to the lower solubility at room temperature. This helps the solder ball to gain ductility as shown in Fig. 7g and j. In  $-25^{\circ}\text{C}$  isothermally aged samples, the maximum shear force ranged with little difference between isothermal aging duration and with a smaller downward trend values associated with longer aging time compared to both room temperature and  $100^{\circ}\text{C}$  aging. The distance to peak shear force plots (Fig. 7i and l) exhibited a similar trend for both strain rates indicating increased ductility with longer  $-25^{\circ}\text{C}$  aging but also with a smaller and slower upward trend. Although the solubility of Bi in Sn is less than the room temperature condition, the limited diffusivity at lower temperature is possibly the reason for this slower response and rate.

A series of EBSD analyses were performed on selected partially sheared solder balls aged for 500 h, as shown in Figs. 8 and 9. Each solder ball was partially sheared up to 70% of the maximum peak shear force then stopped. The comparison of SEM cross section and EBSD results at room temperature (Fig. 8a, b, c, and d),  $100^{\circ}\text{C}$  (Fig. 8e, f, g, and h) and  $-25^{\circ}\text{C}$  (Fig. 8i, j, k, and l) for SAC105 is shown in Fig. 8. A similar comparison was performed for Sn-58Bi at room temperature (Fig. 9a, b, c, d, and e),  $100^{\circ}\text{C}$  (Fig. 9f, g, h, i, and j) and  $-25^{\circ}\text{C}$  (Fig. 9k, l, m, n, and o), presented in Fig. 9. The analyzed EBSD was used to identify the localized grain refinement, locations of developed localized stress and strain regions during shear. For partially sheared SAC105 solder balls, the SEM cross-sectional images revealed the plastically deformed and separation region near the shear tool contact to the solder joint during all temperature conditions, as presented in Fig. 8a, e, and i. The EBSD inverse pole figure (IPF) images in Fig. 8b, f, and j show a grain refinement along the deformation and ball separation region, which is induced by severe plastic deformation. The associated EBSD strain contour maps in Fig. 8c, g, and k also revealed the high-intensity localized strain regions near the solder-to-substrate interface region, specified by white arrows. Along with the EBSD strain contour map, the grain orientation reference deviation (GROD) map presents indirectly the relative residual stress level in relation to adjacent grains, by comparing the level of grain tilting per individual grain versus a grain orientation reference.<sup>14</sup> As displayed in Fig. 8d, h, and i, an increased level of residual stress regions are indicated in the GROD map along the solder-to-substrate interface, which was not yet affected by the shear tool-induced plastic deformation (outlined with boxes A, B and C in Fig. 8c, g, k and d, h, i, respectively). Overall, the results demonstrate that the deformation of these solder joints are fairly ductile.



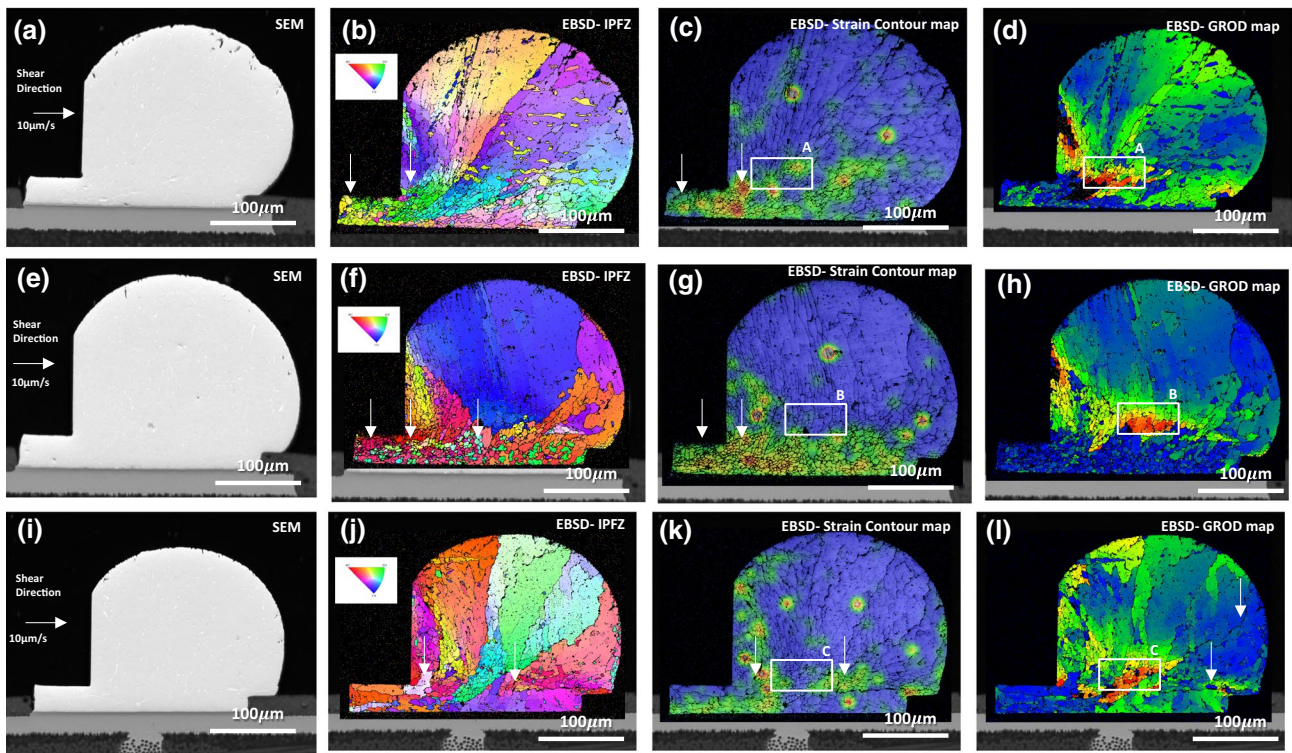


**Fig. 8** SEM and EBSD cross-section microstructure of partially sheared SAC105 solder balls after room temperature aging for 500 h (a, b, c, d), after 100°C/500 h (e, f, g, h), and after -25°C/500 h aging

(i, j, k, l). EBSD inverse pole figure (IPF) images (b, f, j), EBSD strain contour map (c, g, k) and grain reference orientation deviation (GROD) map (d, h, l).

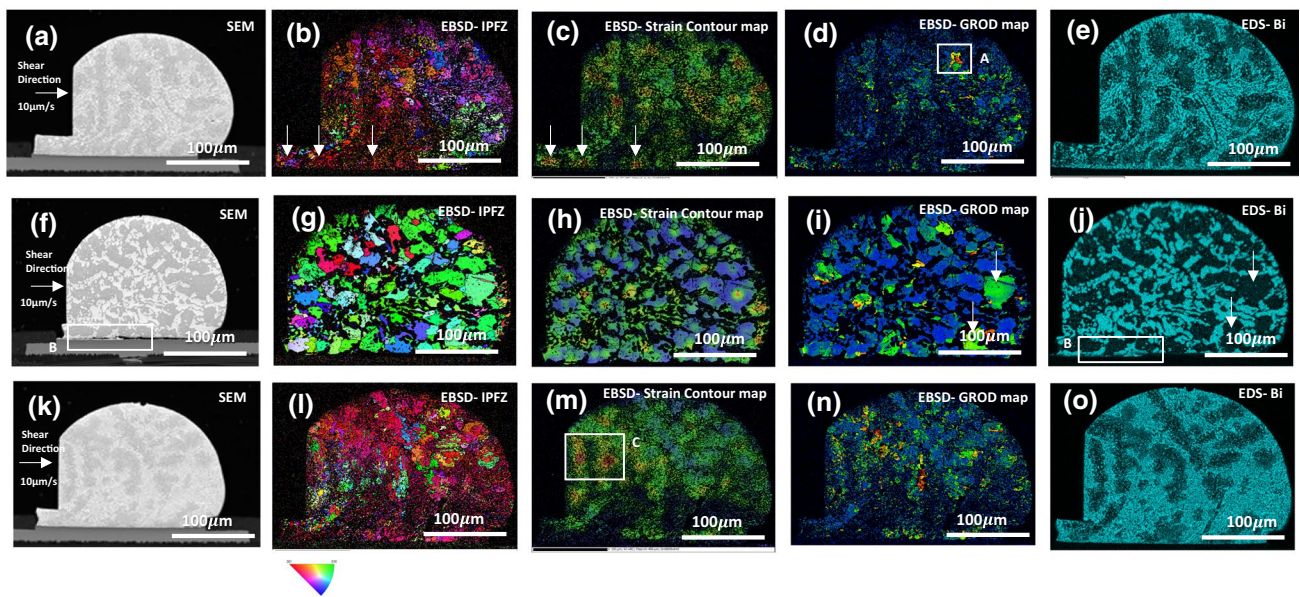


**Fig. 9** SEM and EBSD cross-section microstructure of partially sheared Sn-58Bi solder balls after room temperature aging for 500 h (a, b, c, d, e), after 100°C/500 h (f, g, h, i, j), and after -25°C/500 h aging (k, l, m, n, o). SEM images (a, f, k), EBSD inverse pole figure

(IPF) images (b, g, i), EBSD strain contour map (c, h, m), grain reference orientation deviation (GROD) map (d, i, n), and EDS-Bi map (e, j, o).

The SEM cross section and EBSD inverse pole figure (IPF) images of the Sn-58Bi solder ball sheared at room temperature with 500 h aging are shown in Fig. 9a and b. As indicated by the strain contour map in Fig. 9c with white arrows, high-intensity localized strain was observed near the substrate to the interface area compared to increased strain release in the shear tool contact region. This demonstrates that the interface region retained elasticity and did not introduce plastic deformation. Figure 9d reveals a higher level of residual stress in the solder bulk marked with a white box A in the GROD map. Compared to the partially sheared Sn-58Bi solder ball aged at room temperature, Fig. 9f and k presents the partially sheared solder balls aged at 100°C for 500 h. An increase of grain size is observed and a small shape change on the solder ball showed the different shear behavior compared to the solder ball aged at room temperature. It can be seen that the solder sheared at 100°C was unable to absorb deformation and strain energy due to lack of ductility at a high-temperature environment. As highlighted in Fig. 9f with a white box B, the sample exhibited a crack propagation near the solder-to-IMC interface region as aging resulted in thicker IMC. It is also noticeable that reaching 70% of the maximum shear load required less travel indicating less ductility compared to initial conditions. The same region indicated with box B in Fig. 9j shows a layer of Bi near the interface, which is due to the limitation of Bi solubility into the IMC layer, retaining a layer of Bi near the IMC, from which we can identify it as a transgranular fracture shown in Fig. 4e and f. The brittle nature of Sn-58Bi at elevated temperature was observed through grain size increase as the main solder bulk becomes stiffer and was also demonstrated by the higher level of residual stress regions in Sn grains in Fig. 9i and j shown with white arrows. The higher solubility of Bi into the Sn phase at 100°C resulted in a solid solution hardened Sn-rich grain structure which loses the capability to plastically deform and absorb the shear induced plastic strain, pushing the stress to the interface between the solder ball and IMC interface, resulting in both lower shear force and loss of ductility. Unlike the elevated temperature sheared solder cross section, the sample aged at -25°C revealed localized grain refinement in the Sn region near the substrate-to-solder interface with lower strain intensity and lower residual stress similar to the sample aged at room temperature. However, a small localized strain distribution was observed away from the interface inside the solder in the strain contour map in Fig. 9m, as highlighted with a white box C, while solder-to-substrate revealed a more strain released state. Overall, compared to SAC105 strain contour maps per temperature condition, Sn-58Bi exhibited very well-homogenized strain instead of having very localized strain development.

Given the observation and mechanical shear behavior per condition, the effect of different aging temperatures in

the Sn-58Bi solder on the interfacial morphology can be summarized as follows: Based on the nature of the eutectic system, Bi was the dominant species in Sn-58Bi interdiffusion. The high ambient temperature promotes the solid-solid diffusion in the Sn-58Bi bulks during aging with a higher amount of Bi diffusing into the Sn region, which can be also seen in the Sn-Bi phase diagram (Fig. 1a). On the contrary, aging at RT and -25°C, the diffusion direction of Bi moves towards the Bi bulk itself. Moreover, the diffusion rate is much higher for samples aged at RT for 500 h than that of the sample aged at -25°C, which can be seen in the maximum shear force trend in Fig. 7a and c. In addition, the interfacial IMC layer observed between the solder bulks and Ni/Au substrates in solder joints after aging for 500 h shows a Bi-rich layer since the IMC does not absorb Bi during the development of further (Cu,Ni)<sub>6</sub>Sn<sub>5</sub> layers. Because of the high concentration of Bi in the Sn-58Bi solder and the Bi grain becoming coarsened for samples aged at 100°C, a large number of Bi-rich grains cover the IMC layer on the substrate, which resulted in a more brittle fracture mode as shown in Fig. 4e and f. Therefore, the growth of the IMC layer is suppressed and presents thin and flat morphology in the solder joint.<sup>19</sup> This Bi segregation at high temperature around the SnBi/Ni-Au interface after long-term aging can cause further interfacial embrittlement and can become a crack propagation path.

## Conclusion

Eutectic Sn-Bi solder alloy has a melting temperature of 138°C and thus is the most preferred low-temperature solder interconnect material that lowers thermal warpage-induced defects during assembly. However, it is crucial to understand the mechanical properties of Sn-58Bi solder joints due to the inherent brittleness of the Bi-rich phase, which can cause brittle fracture under mechanical shock and drop conditions for electronic devices. In this study, a shear test method was used to evaluate the solder joint stability of Sn-58Bi solder joints aged for 500 h with NiAu surface finish at room temperature, 100°C and -25°C. Compared to SAC105, which overall shows an increase in ductility, Sn-58Bi samples show an increase in ductility with room temperature isothermal aging, as opposed to a decrease in maximum shear strength and loss of ductility with 100°C isothermal aging. This phenomenon is due to the increased Bi solubility into Sn at higher temperature range. EBSD analysis of partially sheared SAC105 solder joints showed localized deformation in the bulk region at the shear tool contact area, which can absorb the induced strain by plastic deformation. Compared to SAC105, the interface region of isothermally aged partially sheared Sn-58Bi solder joints showed that room temperature shearing was able to retain the elasticity while

shearing at 100°C resulted in the movement of the fracture at the interface between near solder and IMC region where a large amount of coarsened Bi grains diffused. With mechanical shock and drop conditions, the results present the possibility that prolonged isothermal aging induces more brittleness on Sn-58Bi solder interconnects and can have full crack propagation even at low strain rates, which poses a risk the interconnect reliability.

**Acknowledgments** The authors want to thank the Center of Electron Microscopy and Nanofabrication (CEMN) at Portland State University for their technical support on EBSD imaging and analysis. The research leading to these results received funding from the Korea Evaluation Institute of Industrial Technology (KEIT) under grant number 10080187 and by MK Electron.

**Conflict of interest** The authors have no conflicts of interest to declare that are relevant to the content of this article.

## References

1. I. Szendiuch, Development in electronic packaging—moving to 3D system configuration. *Radioengineering* 20, 214 (2009).
2. T. Brandtner, K. Pressel, N. Floman, M. Schultz, and M. Vogl, in *IEEE Electronic Components and Technology Conference (ECTC) Proceedings* (2021), p. 1718
3. G. Chen, X. Zhao, and H. Wu, A critical review of constitutive models for solders in electronic packaging. *Adv. Mech. Eng.* 9, 1 (2017).
4. M. Ribas, T. Hunsinger, T. Cucu, H.V. Ramakrishna, G. Lim, and M. Murphy, *The Printed Circuit Assembler's Guide to Low-Temperature Soldering*, 2nd ed., (California: BR Publishing, 2018).
5. H. Fu, R. Aspandiar, J. Chen, S. Cheng, Q. Chen, R. Coyle, S. Feng, B. Hardin, M. Krmopotich, S. Mokler, J. Radhakrishnan, M. Ribas, B. Sandy, K. Kwan, G. Wu, A. Zhang, and W. Zhen, iNEMI project on process development of BISN-based low temperature solder pastes—part II: characterization of mixed alloy BGA solder joints. in *Pan Pacific Microelectronics Symposium 1* (2018), p. 1
6. H. Kang, S.H. Rajendran, and J.P. Jung, Low melting temperature Sn-Bi solder: effect of alloying and nanoparticle addition on the microstructural, thermal, interfacial bonding, and mechanical characteristics. *Metals* 11, 364 (2021).
7. M. Ribas, A. Kumar, D. Kosuri, R. Rangaraju, P. Choudhury, S. Telu, and S. Sarkar, in *SMTA International Conference and Exhibition Proceedings* (2017), p. 201
8. G. Ren, and N. Collins, Improved reliability and mechanical performance of Ag micro alloyed Sn58Bi solder alloys. *Metals* 9, 462 (2019).
9. M. Ribas, S. Chegudi, A. Kumar, R. Pandher, R. Raut, S. Mukherjee, S. Sarkar, and B. Singh, in *IEEE Electronics Packaging Technology Conference (EPTC) Proceedings* (2014), p. 366
10. H. Lee, K. Choi, Y. Eom, H. Bae, and J.H. Lee, Sn58Bi solder interconnection for low-temperature flex-on-flex bonding. *Electron. Telecommun. Res. Inst. (ETRI)* 38, 1163 (2016).
11. A. Yamaguchi, Y. Fukuhara, A. Behr, H. Hino, Y. Suzuki, and N. Ohashi, in *IEEE Electronic Components and Technology Conference (ECTC) Proceedings* (2017), p. 1398
12. P. Cucka, and C.S. Barrett, The crystal structure of Bi and of solid solutions of Pb, Sn, Sb and Te in Bi. *Acta Cryst.* 15, 865 (1962).
13. O. Chen, J. Gao, T.C.C. Pan, K. Tang, R. Aspandiar, K. Byrd, B. Zhou, S. Mokler, and A. Molina, in *SMTA International conference and Exhibition Proceedings* (2016), p. 2016
14. K. Murayama, M. Aizawa, and T. Kurihara, in *IEEE Electronic Components and Technology Conference (ECTC) Proceedings* (2017), p. 464
15. A. Delhaise, P. Snugovsky, I. Matijevic, J. Kennedy, M. Roman-sky, D. Hillman, D. Adams, S. Meschter, J. Juarez, M. Kammer, I. Straznicki, L. Snugovsky, and D. Perovic, Thermal preconditioning and restoration of bismuth containing, lead free solder alloys. *J. Electron. Mater.* 49, 116 (2020).
16. O. Mokhtari, and H. Nishikawa, Effects of In and Ni addition on microstructure of Sn-58Bi solder joint. *J. Electron. Mater.* 43, 4158 (2014).
17. T.K. Lee, C. Rogan, G. Waduge, Y. Lee, E. Ibe, and K. Loh, in *SMTA International Conference and Exhibition Proceedings* (2020), p. 81
18. A. Kitamura, T. Matthews, R. Contreras, D. Routledge, and T.K. Lee, Impact of cryogenic temperature environment on single solder joint mechanical shear stability. *J. Electron. Mater.* 50, 723 (2020).
19. R. Xu, Y. Liua, and F. Sun, Effect of isothermal aging on the microstructure, shear behavior and hardness of the Sn58Bi/Sn3.0Ag0.5Cu/Cu solder joints. *Results Phys.* 15, 1 (2019).

**Publisher's Note** Springer Nature remains neutral with regard to jurisdictional claims in published maps and institutional affiliations.